EFFECTIVE PERMEABILITY OF DEFORMATION BANDS IN FAULT DAMAGE ZONES – CAN DEFORMATION BANDS REDUCE THE RISK OF FAULT LEAKAGE?

Runar L. Berge[1*], Sarah E. Gasda[1], Eirik Keilegavelin[2], Tor H. Sandve[1]

[1] NORCE, Bergen, Norway

[2] Department of Mathematics, University of Bergen, Bergen, Norway

* Corresponding author e-mail: rube@norceresearch.no

Abstract

Faults are major geological structures that can dominate the flow paths in subsurface reservoirs by, e.g., connecting otherwise unconnected layers. In CO_2 storage sites where the faults act as the main structural trap, the sealing properties of the faults must be fully understood, thus, requiring an accurate representation of the fluid flow close to the faults on all scales. This paper study the effects low permeable deformation bands have on the fluid flow in the near fault region. Deformation bands are generated stochastically, and numerical simulations that include the deformation bands explicitly in the simulation domain are performed to obtain an upscaled effective permeability. The numerical examples show that using a simple harmonic average to calculate the effective permeability may overestimate the effective permeability by up to an order of magnitude. A new analytical approximation of the effective permeability based on the deformation band length, density, and rotation is given, and this approximation fits the numerical simulations better than the harmonic average. The results confirm that deformation bands significantly alter the fluid flow close to faults and may decrease the potential leakage of CO_2 through faults.

Keywords: *Deformation bands – Effective permeability – CO_2 storage integrity – Fault zones – Leakage Risk*

1. Introduction

Fluid flow and migration in sedimentary basins have for centuries been a challenge to modelling in a variety of applications, such as groundwater management, hydrocarbon production [1], and recently CO_2 storage [2]. To implement large-scale CO_2 storage, a wide range of reservoir types must be exploited, including reservoirs where faults form the main structural trapping mechanism. A challenge with faults as structural traps is to validate their sealing potential due to the difficulty to predict the properties of the faults. For hydrocarbon reservoirs the fault sealing can be validated by drilling exploratory wells to confirm the existence of hydrocarbons, whereas this is not applicable to aquifers. Mitigating risks related to fault sealing by improving our understanding of the broad range of fluid flow dynamics around faults is therefore needed to unlock storage reservoirs where faults form the main structural trapping mechanism for CO_2.

Fluid flow around faults is governed by geometrically complex structures at a range of scales. There are two different fluid paths that are important to characterize with respect to fault leakage and loss of containment of CO_2. We divide these two paths into the vertical fluid flow along the slip surface in the fault core, and horizontal fluid flow across the fault, see Figure 1 for a conceptual model. The Shale Gouge Ratio of a fault has been identified as a controlling parameter for the sealing properties of faults [3], and the current state-of-the art fault-seal analysis [4] are developed around the shale content as a controlling parameter. However, these methods only capture across-fault flow [5, 6] and not the complexity of the damage zone or fluid flow vertically along faults.

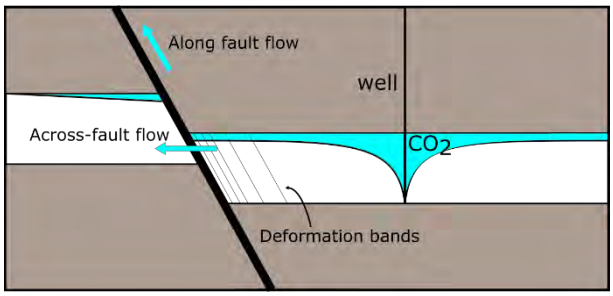

Figure 1: Conceptual model of two possible leakage paths of CO_2 when faults form the main structural trapping mechanism; across-fault flow and along fault flow. Deformation bands that form parallel to the fault may reduce both across-fault flow and along-fault flow by reducing the effective permeability.

One of the structures that is found in the damage zone is deformation bands, which are millimeter-thick low-displacement deformation zones [7]. Deformation bands can have a one to six orders of magnitude lower permeability than the host rock [8, 7, 9], which has led to investigations regarding the impact of deformation bands on fluid flow [10, 11, 12]. These studies have shown that deformation bands can alter the fluid flow paths in a

reservoir, especially if the permeability contrast is lower than four orders of magnitude, but also if the permeability contrast is as low as one order of magnitude [13]. The number of deformation bands around a fault can be related to fault throw [14] and can reach tens of bands per meter close to the fault core. In a potential storage site for CO_2 the individual deformation bands will be unknown and their distribution must be derived from analogue outcrops and models. A quantity that is possible to measure on seismic imaging is the throw of a fault. This triggers the question if it is possible to quantify the effects of deformation bands based on the fault throw. In this paper we give insight into how geometric parameters of the deformation bands impact fluid flow within the damage zone around faults and relate these to fault throw. We do this by generating deformation bands stochastically using recent quantifications of deformation bands in the damage zone [14], and upscale the effective permeability of the generated networks by numerical simulations and analytical approximations.

The Smeaheia storage prospect in the North Sea is considered as a possible storage site for CO_2 [15]. The site is confined by the Vette fault which is predicted to be a structural trap. Including deformation bands in a reservoir scale model will improve our understanding of the fluid flow around the Vette fault and help mitigate the leakage risks of the Smeaheia storage site. In reservoir scale simulations, the size of grid cells is typically on the order of 10 m to 100 m, while the length of the deformation bands is on the order of 10 cm to 100 m. Further, the aperture of the deformation bands is on the millimeter scale. This makes it clear that it is impossible to include deformation bands explicitly in a reservoir scale simulation. Instead, the deformation bands are typically included by considering an effective permeability that represents the combined permeability of the deformation bands and the host rock. This will in general lead to an anisotropic permeability tensor because of the geometric structure of the deformation bands [16]. The effectiveness of this approach is dependent on how well the effective permeability is estimated. An approach that has been used to calculate the effective permeability of the combined porous media of deformation bands and host rock is by a harmonic averaging procedure [12]. While this gives a lower bound on the effective permeability, it will miss the contribution of the geometry of the deformation bands, which has the potential to affect the fluid flow in complicated manners.

The main contributions of this work are twofold. First, we propose a new analytical model for the effective permeability that includes geometry effects of the deformation bands. The derived expression can be used to calculate the effective permeability in other geological settings than around faults, however, this paper only validates the model with data generated from fault zones. Secondly, we perform fine-scale numerical simulations of fluid flow that resolve individual deformation bands explicitly in the simulation domain. In this study we vary the band permeability, band geometry, and band density to investigate how the different parameters affect the effective permeability in the damage zone around faults.

The remainder of the paper is outlined as follows. The next section discusses the geometric setup and how this relates to faults. Section 3 defines the governing equations for single-phase flow, and Section 4 presents the numerical method used to solve the governing equations with explicitly represented deformation bands in the domain. Section 5 presents our new approximation of the effective permeability and validates it against cases where the band density is constant in the domain. Section 6 contains the main results of this paper, a parameter study of the effective permeability in the damage zone of faults. Here we compare both the numerical simulations and the proposed analytical approximation from Section 5. The final section contains discussion and conclusions.

2. Geometric setup

Deformation bands are thin surfaces that close to a fault tend to form parallel to the fault. While the horizontal extent of the deformation bands can vary from centimeters to hundreds of meters, the deformation bands are often bedding constrained in vertical direction [17, 18]. To reduce the computational cost, we therefore collapse the vertical dimension of the permeable layer and run simulations on two-dimensional domains.

In this work, the deformation bands are generated stochastically by a similar procedure as described in [19]. Deformation bands are represented by straight-line segments, and the line segments can be described by the band centers and the rotations from the y-axis, θ, both stochastic variables. The distributions will be specified in each section. The length of the bands is denoted by l, and the band density, ρ, is defined as the expected number of band centers per unit area. Similarly, the directional density, ρ_α, is defined as the expected number of bands intersecting a scan-line per unit length in the direction α.

3. Governing equations

We consider an incompressible single-phase fluid in a porous media. The porous media consists of two materials, the host rock and the deformation bands. Quantities related to the host rock are denoted by a subscript m and quantities related to the deformation bands are denoted by a subscript b. The permeability within the host rock and deformation bands are assumed to be each homogenous and isotropic and defined by the scalars, k_m and k_b, respectively. The fluid flux, $\boldsymbol{q}$, is related to the pressure, p, through Darcy's law. Together with conservation of mass this defines our governing equations:

$$\boldsymbol{q} = -k\nabla p, \quad \nabla \cdot \boldsymbol{q} = 0,$$

where $k = k_m$ in the host rock and $k = k_b$ in the deformation bands. In addition, we assume appropriate boundary conditions to be defined.

Lower-bound on effective permeability

A lower-bound of the effective permeability, $K_{\alpha,e}$, can be obtained by taking the harmonic average of the deformation band permeability and the host rock permeability along the scanline α:

$$\frac{K_{\alpha,e}}{K_m} \geq \frac{1}{(1-\rho_\alpha a)+\frac{\rho_\alpha a K_m}{K_b}} \approx \frac{1}{1+\frac{\rho_\alpha a K_m}{K_b}}. \qquad (1)$$

Here, a, is the aperture of the deformation bands. This lower-bound is obtained if the fluid is not able to flow around the deformation bands but must cross all bands that intersect the scanline in the direction α. In the numerical results we observe that the lower bound is approached as the band length and/or band density increases.

The error of the approximation in Equation (1) is small if $\rho_\alpha a \ll 1$. Out of the 106 outcrop scanlines studied in [14] none of the scanlines had a maximum band density of more than 110 bands per meter, with the mean being 34 bands per meter. If the deformation bands have an aperture $a \approx 1$ mm, the error of the approximation is small. When $\rho_\alpha a \ll 1$, we observe that the reduction in permeability given by the harmonic average in Equation (1) is only dependent on the dimensionless quantity $\rho_\alpha a K_m / K_b$. Thus, a single dimensionless quantity may describe the effect of the deformation bands! Finally, when the density is varying in the domain the averaged value should be used. Specifically, for the logarithmic density in Section 6 (Equation (4)), the density in Equation (1) can be replaced by $-B$.

4. Numerical method

Before we describe the numerical method, we would like to make two comments. The aperture of the deformation bands, a, is typically on the order of magnitude of milli meters, while their lengths can span up to several hundred meters [7]. In addition, the permeability in the deformation bands, k_b, is lower than the permeability in the host rock. We will therefore disregard the fluid flux in the tangential direction of the deformation bands. To represent the permeability reduction caused by the deformation bands, the computational grids are constructed to conform to the bands. That is, the deformation bands will be discretized by the faces in the computational grid. To discretize the governing equations, we use the two-point flux approximation. The two-point flux approximation is sufficient for our purposes because we are only interested in the reduction in effective permeability relative to the homogeneous case. In addition, we are using a completely unstructured grid that reduces the consistency error. By neglecting the tangential flow, assuming small apertures, and using a conforming grid, the deformation bands can be included in the discretization as a face transmissibility multiplicator, as described in the following paragraphs.

Let σ be a face between cell L and cell R. The fluid flux from cell L to cell R is approximated by

$$F_\sigma = -T_\sigma(p_R - p_L),$$

where T_σ is the transmissibility and p_R and p_L are the cell center pressure. If the face between the cells do not lie on a deformation band the transmissibility is calculated by the harmonic average of the two half transmissibilities:

$$T_\sigma = \frac{T_{\sigma L} T_{\sigma R}}{T_{\sigma L} + T_{\sigma R}}, \quad T_{\sigma k} = \frac{k_m A_\sigma \boldsymbol{n}_{\sigma k} \cdot \boldsymbol{d}_{\sigma k}}{\boldsymbol{d}_{\sigma k} \cdot \boldsymbol{d}_{\sigma k}}, \quad k \in \{L, R\}.$$

Here, A_σ is the area of the face, $\boldsymbol{n}_{\sigma k}$ is the unit normal vector of σ that points out of cell k, and $\boldsymbol{d}_{\sigma k}$ is the distance vector from the cell center to the face center. If the face is on a deformation band, the transmissibility is modified to include the effect of the bands by taking the harmonic average of the band transmissibility and the half transmissibility of each cell:

$$T_\sigma = \frac{T_{b\sigma L} T_{b\sigma R}}{T_{b\sigma L} + T_{b\sigma R}}, \quad T_{b\sigma k} = \frac{k_b T_{\sigma k}}{k_b + \frac{T_{\sigma k} a}{2A_\sigma}}, \quad k \in \{L, R\}.$$

5. Layered approximation of the effective permeability

In this section we propose a new approach to estimate the effective permeability. This approach approximates the effective permeability in the domain by using some well-educated simplifications. In this section we assume that the band density, ρ, is constant in the domain.

When the fluid approaches a deformation band, parts of the fluid will cross the band and parts of the fluid will flow around the band. The effective permeability is approximated by considering the path across the band and the path around the band as a layered porous media with two layers. This conceptual model is depicted in Figure 2 for fluid flow in the x-direction.

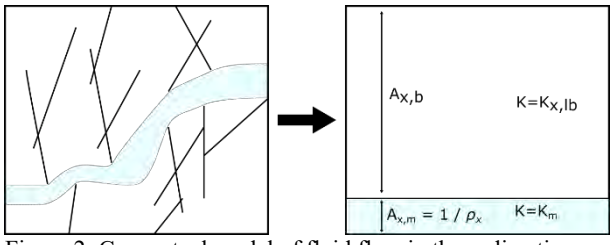

Figure 2: Conceptual model of fluid flow in the x-direction. The complex geometry of the deformation bands is simplified to an area where the fluid only flow through the rock matrix (blue), and an area where the fluid crosses the deformation bands (white).

Given the conceptual model of the porous media consisting of two layers, the effective permeability in the direction α can be calculated as

$$K_{\alpha,e} = \frac{K_{\alpha,lb} A_{\alpha,b} + K_m A_{\alpha,m}}{A_{\alpha,b} + A_{\alpha,m}}, \qquad (2)$$

where $A_{\alpha,b}$ and $A_{\alpha,m}$ are the areas available for flow in the band layer and host rock layer, respectively (see Figure 2). The permeability in the band layer, $K_{\alpha,lb}$, is obtained by calculating the harmonic mean of the band

permeability and rock matrix permeability, using the approximation of small band aperture:

$$\frac{K_{\alpha,lb}}{K_m} = \frac{1}{1 + \frac{K_m a \rho_\alpha}{K_b} c_\alpha}.$$

Here, the constant c_α defines the fraction of the number of bands within the band layer the fluid must cross. When the rotation of the bands is normally distributed, $\theta = \mathcal{N}(0, \sigma)$, we use

$$c_x = 1, \;\; c_y = \sin\left(E(|\theta|)\right),$$

where $E(|\theta|)$ is the expected value of the absolute value of the rotation. The challenging part of this approach is to obtain good estimates on the area available for flow around, $A_{\alpha,m}$, and across, $A_{\alpha,b}$, the deformation bands, and the remaining of this section will focus on this.

Let us consider an arbitrary deformation band, called r. Each other deformation band in the domain has a certain fixed probability of crossing this band. When ρ is independent of position and the bands are independently distributed, the number of intersections, N, band r has with other bands is Poisson distributed. The probability of the band having zero intersections can be calculated as

$$P(N = 0) = \exp\left(-l^2 \rho \int_{-\infty}^{\infty} \int_{-\infty}^{\infty} |\sin(\theta)| \, f(\theta + \eta) f(\eta) \mathrm{d}\theta \mathrm{d}\eta\right),$$

where $f(\theta)$ is the probability density function of the rotation of the bands. If the rotation of the bands is uniform, the integral simplifies to $2/\pi$. If the rotation of bands is normally distributed the integral can be calculated numerically. Since N is Poisson distributed, the expected value can be calculated as

$$E(N) = -\log\left(P(N = 0)\right). \qquad (3)$$

Figure 3 shows a comparison of the Poisson distribution with expectation $E(N)$ and the probability density function calculated numerically by populating a domain with 10 000 deformation bands stochastically. The fit is good and gives no reasons to doubt that the number of intersections is Poisson distributed with expected value given by Equation (3).

Let M denote the number of bands you must pick at random before picking a band with 0 intersections. The expected value of M can be calculated as:

$$E(M) = \frac{1 - P(N = 0)}{P(N = 0)^2}.$$

When the deformation bands intersect, they may form long chains of bands. When a band is added to the chain the chain grows in a random direction, and we postulate that the growth of the chain follows the same scaling as Brownian motion, that is, the length grows with the square root of the number of bands. We have confirmed this scaling numerically. We therefore suggest that the area available for flow across deformation bands is

$$A_{\alpha,b} = l_\alpha^\top + \sqrt{0.5 \, l_\alpha^\top \, E(M)}.$$

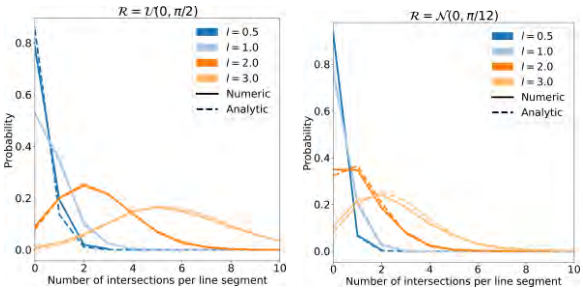

Figure 3: The probability of a band having N intersections. The solid lines show the probability calculated numerically by distributing 10 000 bands randomly in a domain, while the dashed lines show the Poisson distribution. In the left figure the band rotation is uniformly distributed, while in the right figure the band rotation is normally distributed.

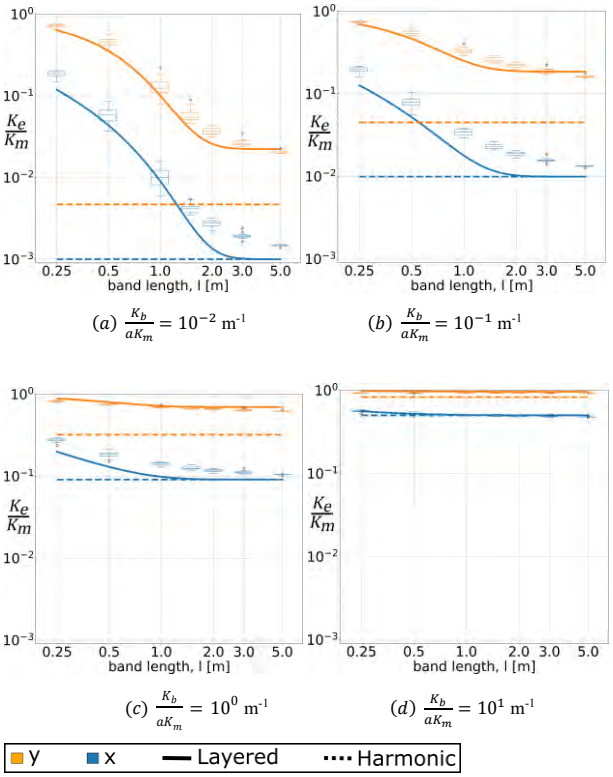

Figure 4: The effective permeability (y-axis) as a function of the band length (x-axis) for a band density independent of position in the domain. The box plots show the effective permeability obtained from numerical simulations, the solid lines correspond to the effective permeability obtained by the layered analytical approximation, and the dashed lines to the harmonic average. The orange color corresponds to the effective permeability in y-direction, while the blue color corresponds to the effective permeability in x-direction. Each figure shows the result of a different permeability ratio of the rock matrix and the deformation bands.

Here, $l_\alpha^\top$, is the expected band length in the direction perpendicular to α. If the rotation is normally distributed with standard deviation σ, $\mathcal{R} = \mathcal{N}(0, \sigma^2)$, and $\sigma \ll 1$, we obtain

$$l_x^\top = l \cos\left(\frac{\sigma\sqrt{2}}{\pi}\right), \; l_y^\top = l \sin\left(\frac{\sigma\sqrt{2}}{\pi}\right), \; \rho_\alpha = \rho l_\alpha^\top.$$

For the conceptual layer of the host rock, the area available for flow is the area between bands. We

therefore suggest that the area for the host rock in our conceptual model scales as

$$A_{\alpha,m} = 1/\rho_\alpha.$$

Comparison to numerical simulations

To test the suggested analytical solution for the effective permeability as a layered porous media we compare the analytical approximation given by Equation (2) to the effective permeability calculated from the numerical simulations. We let $\mathcal{R} = \mathcal{N}(0, (\pi/12)^2)$ and fix the density to $\rho = 1$ m^{-2}. The band length, l, is varied between 0.25 m and 5 m. The comparisons between the analytical approximations and numerical solutions are shown in Figure 4. Using the harmonic average approximation given by Equation (1) consistently underestimates the permeability; up to two orders of magnitude in the worst case. The analytical approximation given by Equation (2) gives a much better approximation and is able to capture the increase in effective permeability as the deformation band network becomes disconnected. Finally, we note that as the deformation band length increases or the permeability ratio decreases, the error of the harmonic average becomes smaller.

Figure 5 shows the comparison of the numerical simulations and the analytical approximation as a function of band density, ρ. The band length is fixed to $l = 1$ m. The analytical approximation of the effective permeability given by Equation (2), is able to capture the effective permeability both when the band network is disconnected (the band density small), and when it is highly connected (band density is large), while the harmonic average given by Equation (1) is only applicable when the band density or the band transmissibility, $\frac{K_f}{aK_m}$, is large. This is the same qualitative behavior as observed in Figure 4.

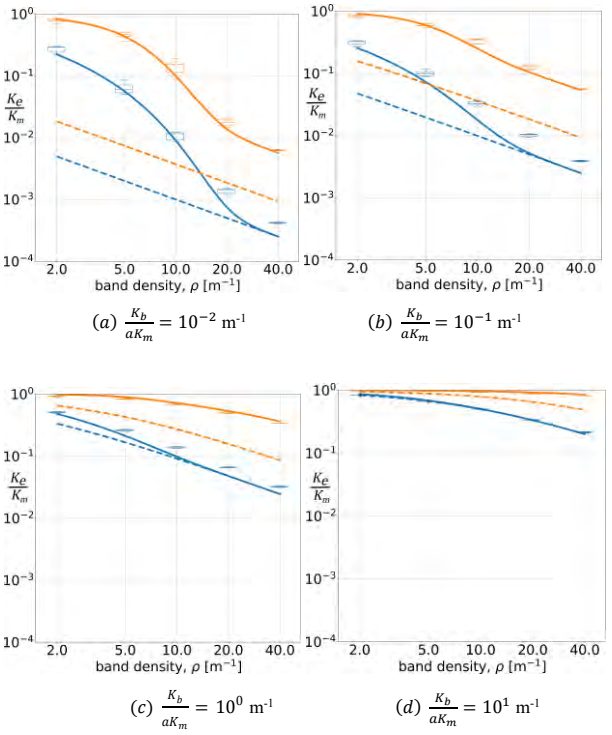

Figure 5: The effective permeability (y-axis) as a function of the band density (x-axis) for a density that is independent of position in the domain. The box plots show the effective permeability obtained from numerical simulations, the solid lines correspond to the effective permeability obtained by the layered analytical approximation, and the dashed lines to the harmonic average. The orange color corresponds to the effective permeability in y-direction, while the blue color corresponds to the effective permeability in x-direction. Each figure shows the result of a different permeability ratio of the rock matrix and the deformation bands.

6. Application to fault damage zones

Around faults the number of deformation bands is not constant but varies as a function of the distance from the fault. In this section we assume the density function along a scanline normal to the fault (x-direction) follows the logarithmic law given in [14]:

$$\rho_x(x) = A + B \ln\left(\frac{x}{1\text{m}}\right), \qquad (4)$$

where A and B are two constants that can be used to fit the density function to a specific fault. We will use the average values from the data given in [14]:

$$B = -8.33 \text{ m}^{-1},$$

$$A = 13.33 \ln\left(\frac{W_5}{1\text{ m}}\right) \text{m}^{-1} - 5\left(\ln\left(\frac{W_5}{1\text{ m}}\right) - 1\right) \text{m}^{-1},$$

where W_5 is the distance from the fault to where the band frequency is 5 m^{-1}, that is $\rho(W_5) = 5$ m^{-1}. We refer to this value as the damage zone width. The damage zone width can be related to fault throw, T, as (see [14])

$$W_5 = 1.74 \left(\frac{T}{1\text{ m}}\right)^{0.43} \text{m},$$

which allows us to generate deformation band networks based on only the fault throw.

Figure 6 shows three examples of generated deformation band networks using the logarithmic density function. The figure illustrates that increasing values of W_5 both widens the damage zone and increases the frequency of the bands within the zone. The deformation zone widths are 1 m, 5 m, and 10 m, which correspond to fault throws of 0.28 m, 12 m, and 58 m, respectively.

The analytical expression using the approximation of the effective permeability given in Equation (2) was derived for domains where the density was constant, however, if the density is varying slowly enough, we expect that Equation (2) gives a good point estimate of the effective permeability. By integrating the point estimate of the effective permeability, the effective permeability of the whole domain can be obtained.

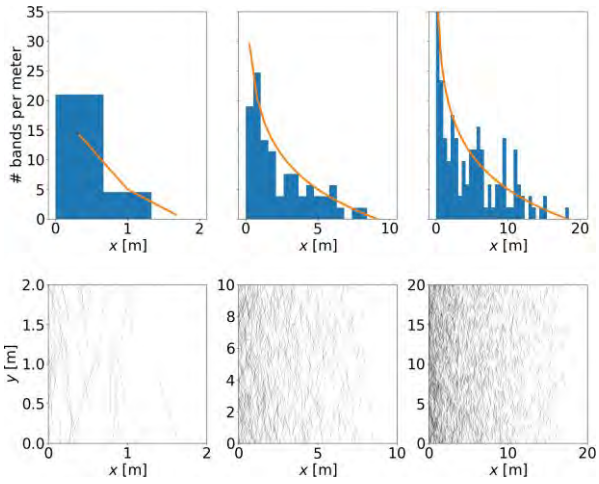

Figure 6: Example of three generated deformation bands networks that follow the logarithmic density function (bottom row). The damage zone width is $W_5 = 1, 5,$ and 10 meters from the left figure to the right figure. The top row shows the histograms of the deformation bands crossing the horizontal scan line through the center of the domain, while the orange line shows the density function given by Equation (4). The fault is parallel to the y-axis and located at $x = 0$. Note the different axis is each plot.

We will test the analytical approximation by comparing it to numerical simulations. Three tests are performed, varying the parameters going into the model independently.

Common setup

The following parameters are used in all the following examples. The coordinate system is chosen such that the fault is parallel to the y-axis, and the x-axis defines the distance from the fault. In the numerical simulations the effective permeability in x- (resp. y-) direction is calculated by imposing a unit drop in pressure in x- (resp. y-) direction and imposing a no-flow condition on the top and bottom (resp. left and right) boundaries.

The computational domain is a square, $[X, Y]$. The height, Y, is set is set to 8 times the band length. This domain height has been found to be sufficiently large so that a doubling of the domain height does not alter the results. The domain width, X, is set equal the width at which no deformation appears, that is, $\rho_x(X) = 0$.

In all test cases the band transmissibility is defined as the permeability ratio divided by the aperture. In each test case the band transmissibility is varied four orders of magnitudes, $\frac{K_b}{aK_m} = \{10^{-2}, 10^{-1}, 10^{0}, 10^{1}\}$ m^{-1}. The lowest band transmissibility corresponds to, e.g., an aperture of 1 mm and permeability ratio of 5 orders of magnitude.

In all test cases the rotation of the bands, θ, is assumed normally distributed with standard deviation σ, $\mathcal{R} = \mathcal{N}(0, \sigma^2)$.

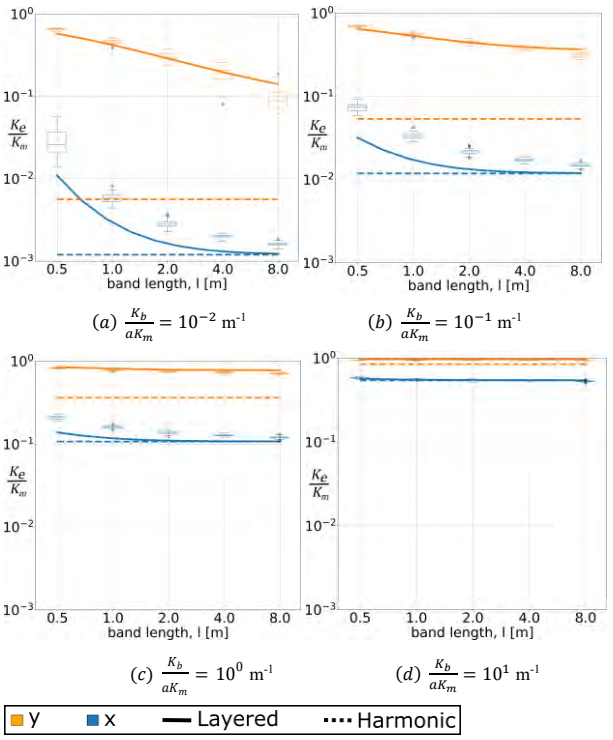

Figure 7: The effective permeability of the fault damage zone as a function of the band length. The box plots show the effective permeability obtained from numerical simulations, the solid lines correspond to the effective permeability obtained by the layered analytical approximation, and the dashed lines to the harmonic average. Blue color is the permeability normal to the fault, while the orange color is the permeability parallel to the fault.

6.1 Effective permeability vs. band length

In this test, the damage zone width is fixed to $W_5 = 5$ m, which corresponds to a throw of 12 m. The standard deviation of the rotation is set to $\sigma = \pi/12$. The band length is varied between simulations and takes values 0.5, 1, 2, 4, and 8 meters. For each band length a total of 48 simulations were run.

Figure 7 shows the effective permeability in x- and y-direction as a function of band length. As the length of the bands increase, the effective permeability approaches the lower-bound given by the harmonic average in Equation (1). The layered approximation in Equation (2) gives quite good match with the numerical results. We observe that the effective permeability varies an order of magnitude between band lengths of 0.5 m and band lengths of 4.0 m and has an anisotropy up to two orders of magnitude in the normal and parallel directions.

6.2 Effective permeability vs rotation

In this test case the expected band length is fixed to $l = 1$ m, and the damage zone width to $W_5 = 5$ m. Varying the standard deviation in the normal distribution, σ, changes how much the deformation bands intersect. When the standard deviation is 0 all bands are parallel, and no bands intersect. When the standard deviation is more than $\pi/5$ there is not much structure in the deformation bands and the generated network resembles that of a uniform distribution. In the numerical tests, we consider this full range of rotations. For each value of σ

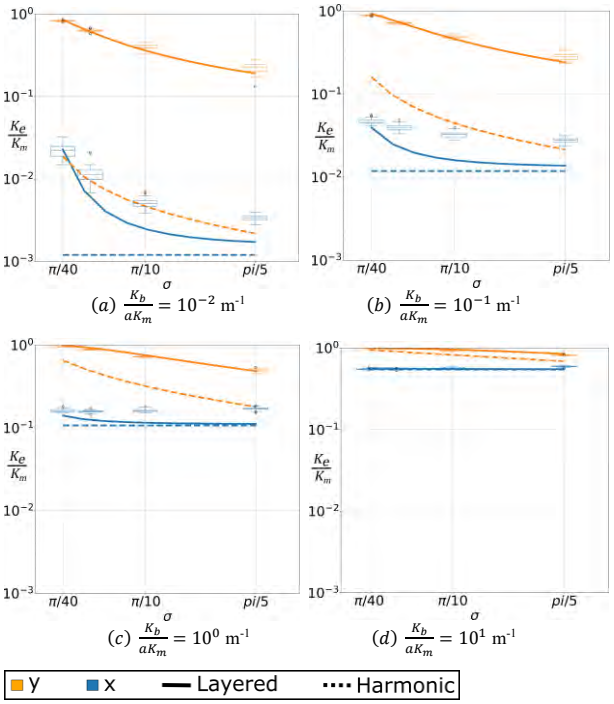

Figure 8: The effective permeability of the fault damage zone as a function of the band rotation. Each subplot shows the result for a different permeability ratio. The box plots show the effective permeability obtained from numerical simulations, the solid lines correspond to the effective permeability obtained by the layered analytical approximation, and the dashed lines to the harmonic average. Blue color is the permeability normal to the fault, while the orange color is the permeability parallel to the fault.

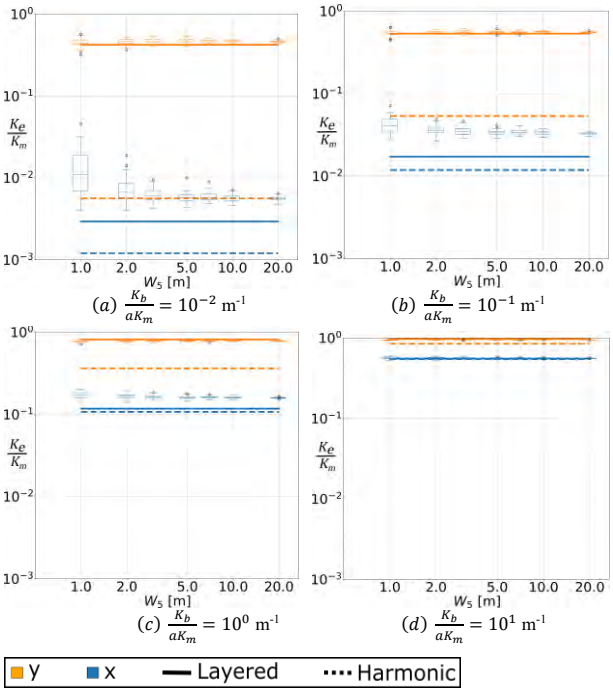

Figure 9: The effective permeability in the damage zone as a function of damage zone width. Each subplot shows the result for a different permeability ratio. The box plots show the effective permeability obtained from numerical simulations, the solid lines correspond to the effective permeability obtained by the analytical approximation, and the dashed lines to the harmonic average. Blue color is the permeability normal to the fault, while the orange color is the permeability parallel to the fault.

a total of 48 realizations of the deformation band network was created.

Figure 8 shows the effective permeability for each case. The effective permeability decreases as the rotation increases because the bands tend to intersect each other more which creates long connected chains of deformation bands that the fluid must cross. The permeability parallel to the fault is approximately 2 orders of magnitude larger than the permeability normal to the fault for the fault transmissibility 10^{-2} m^{-1}, but decreases as the fault transmissibility increases.

6.3 Effective permeability vs damage zone width, W_5

We upscale the effective permeability for the damage zone widths W_5 = 1, 2, 3, 5, 7, 10, 20 meters numerically by generating 48 realizations of the deformation bands for each length. These damage zone widths correspond to a throw of 0.28, 1.4, 3.5, 12, 25, 58 and 293 meters, respectively.

The effective permeability is plotted in Figure 9. The variance of the effective permeability decreases with increasing damage zone width, however, the value of the effective permeability appears to be constant. That the effective permeability is independent of fault throw is also predicted by both the harmonic average approximation in Equation (1), and the layered approximation in Equation (2). The reason for this is that the choice of A and B causes the total number of deformation bands in the domain divided by the damage zone width to be constant. That band density averaged over the damage zone is independent of damage zone width is consistent with field observations [14]. This causes the width of the damage zone to increase at the same rate as the number of bands in the damage zone. Thus, the changes in these two parameters cancel each other in the calculation of the effective permeability. Note that this is only true for the effective permeability averaged over the whole damage zone; the point value of the effective permeability, e.g., 1 m from the fault is much lower for a fault throw of 300 m than a fault throw of 2 m.

8. Discussion and conclusion

In this paper a novel analytical expression for the effective permeability of a porous media with deformation bands is presented. The analytical expression assumes the porous media can be represented as two layers, one with deformation bands and one without. The analytical solution is validated by numerical simulations over a wide range of parameters.

The results from the numerical simulations show that deformation bands can significantly alter the effective permeability in the damage zone of faults. It is also

shown that the geometry of the deformation bands is important when estimating the effective permeability. Counting the number of deformation bands along a scan line from a fault and taking the harmonic average between the deformation bands and host matrix can overestimate the reduction in permeability by an order of magnitude. The main mechanism that increases the effective permeability is that the geometry allows the fluid to bypass bands without crossing them. This effect is especially important when the permeability ratio of the deformation bands and the rock matrix is smaller than three orders of magnitude.

In the results presented in this paper it is assumed that deformation bands are placed randomly in the domain by a stochastic process and that each deformation band is independent of all others. This is an assumption that not necessary holds true for a field case, and an important part of further work will be to quantify the difference between the proposed method and field observations. In this work it will be necessary to explore appropriate methods for including the suggested model in a reservoir simulation. The discrepancy in scales between the damage zone and grid cell size may cause a straightforward upscaling of the grid cell permeability to underestimate the effects of the bands. Special care should then be taken close to faults where, due to the logarithmic density function of deformation bands, the deformation band density varies significantly, and a representative elementary volume of the combined deformation bands and host rock may not exist.

Acknowledgements

This work has been founded in part by the Norwegian Research Council grant 294719.

References

[1] D. Faulkner, C. Jackson, R. Lunn, R. Schlische, Z. Shipton, C. Wibberley and M.O. Withjack, "A review of recent developments concerning the structure, mechanics and fluid flow properties of fault zones," *Journal of Structural Geology,* vol. 32, no. 11, pp. 1557-1575, 2010.

[2] F. Cappa and J. Rutqvist, "Modeling of coupled deformation and permeability evolution during fault reactivation induced by deep underground injection of CO2," *International Journal of Greenhouse Gas Control,* vol. 5, no. 2, pp. 336-346, 2011.

[3] Y. Pei, D. A. Paton, R. J. Knipe and K. Wu, "A review of fault sealing behaviour and its evaluation in siliciclastic rocks," *Earth-Science Reviews,* vol. 150, pp. 121-138, November 2015.

[4] R. J. Knipe, "Juxtaposition and Seal Diagrams to Help Analyze Fault Seals in Hydrocarbon Reservoirs," *AAPG Bulletin,* vol. 81, no. 2, pp. 187-195, 1997.

[5] A. Braathen, J. Tveranger, H. Fossen, T. Skar, N. Cardozo, S. E. Semshaug, E. Bastesen and E. Sverdrup, "Fault facies and its application to sandstone reservoirs," *AAPG Bulletin,* vol. 93, no. 7, pp. 891-917, 2009.

[6] M. Fachri, J. Tveranger, A. Braathen and P. Røe, "Volumetric faults in field-sized reservoir simulation models: A first case study," *AAPG Bulletin,* vol. 100, no. 5, pp. 795-817, 2016.

[7] H. Fossen, R. Schultz, Z. Shipton and K. Mair, "Deformation bands insandstone - a review," *Journal of the Geological Society,* vol. 164, no. 4, pp. 755-769, 2007.

[8] M. Antonellini and A. Aydin, "Effect of faulting on fluid flow in poroussandstones: petrophysical properties," *AAPG Bulletin,* vol. 78, no. 3, pp. 355-377, 1994.

[9] G. Ballas, R. Soliva, J.-P. Sizun, A. Benedicto, T. Cavailhes and S. Raynaud, "The importance of the degree of cataclasis in shear bands for fluid flowin porous sandstone, Provence, France," *AAPG Bulletin,* vol. 96, no. 11, pp. 2167-2186, 2012.

[10] S. Matthäi, A. Aydin, D. Pollard and S. Roberts, "Numerical simulation of departures from radial drawdown in a faulted sandstone reservoir with joints and deformation bands," in *Faulting, fault sealing and fluid flow in hydrocarbon reservoirs*, G. Jones, Q. Fisher and R. Knipe, Eds., London, Geological Society, Special Publications, 1998, pp. 157-191.

[11] K. Sternlof, J. Chapin, D. Pollard and L. Durlofsky, "Permeabilityeffects of deformation band arrays in sandstone," *AAPG Bulletin,* vol. 88, no. 9, pp. 1315-1329, 2004.

[12] H. Fossen and A. Bale, "Deformation bands and their influence on fluid flow," *AAPG Bulletin,* vol. 91, no. 12, pp. 1685-1700, 2007.

[13] A. Rotevatn, H. S. Fossmark, E. Bastesen, E. Thorsheim and A. Torabi, "Do deformation bands matter for flow? Insights from permeabilitymeasurements and flow simulations in porous carbonate rocks," *Petroleum Geoscience,* vol. 23, no. 1, p. 104–119, 2017.

[14] S. Schueller, A. Braathen, H. Fossen and J. Tveranger, "Spatial distribution of deformation bands in damage zones of extensional faults in porous sandstones: Statistical analysis offield data," *Journal of Structural Geology,* vol. 52, pp. 148-162,, 2013.

[15] OED, "Feasibility study for full-scale CCS in Norway," 09 2019. [Online]. [Accessed 19 02 2021].

[16] K. R. Sternlof, M. Karimi-Fard, P. D. D. and L. J. Durlofsky, "Flow and transport effects of compaction bands in sandstone at scales relevant to aquifer and reservoir management," *Water Resources Research,* vol. 42, no. 7, p. W07425, 2006.

[17] R. A. Schultz and H. Fossen, "Displacement–length scaling in three dimensions: the importance of aspect ratio and application to deformation bands," *Journal of Structural Geology,* vol. 24, no. 9, pp. 1389-1411, 2002.

[18] M. L. Cooke and C. A. Underwood, "Fracture termination and step-over at bedding interfaces due to frictional slip and interface opening," *Journal of Structural Geology,* vol. 23, no. 2-3, pp. 223-238, 2001.

[19] C. Xu and P. Dowd, "A new computer code for discrete fracture network modelling," *Computers & Geosciences,* vol. 36, no. 3, pp. 292-301, 2010.

[20] A. Aydin, R. Borja and P. Eichhubl, "Geological and mathematical frameworkfor failure modes in granular rock," *Journal of Structural Geology,* vol. 28, no. 1, pp. 83-98, 2006.